Transition Induced by Fence Geometries on Shuttle Orbiter at Mach 10

Joel L. Everhart*
NASA Langley Research Center, Hampton, VA, 23681

Fence-induced transition data simulating a raised gap filler have been acquired on the wing lower surface of a Shuttle Orbiter model in the Langley 31-Inch Mach 10 Tunnel to compare with the Shuttle Boundary Layer Transition Flight and HYTHIRM Experiments, and to provide additional correlation data for the Boundary Layer Transition Tool. In a qualitative assessment, the data exhibit the expected response to all parameter variations; however, it is unclear whether fully effective tripping at the fence was ever realized at any test condition with the present model hardware. A preliminary, qualitative comparison of the ground-based transition measurements with those obtained from the STS-128 HYTHIRM imagery at Mach 15 reveal similar transition-wake response characteristics in terms of the spreading and the path along the vehicle surface.

Nomenclature

h	heat transfer coefficient, $h=q/(H_{aw}-H_w)$, $(lbm/ft^2/s)$
k	trip or fence height
L, W, H	fence length, width, and depth (in)
M	freestream Mach number
M_e	boundary layer edge Mach number at the fence
Re	Reynolds number based on model length
Re_{kk}	roughness Reynolds number based on height k and conditions at k
Re_θ	momentum thickness Reynolds number at the fence
x	axial distance from model leading edge (in)
y	spanwise distance from model centerline (in)
z	distance normal to x-y plane (in)
α	angle-of-attack (deg)
β	yaw angle (deg)
δ	boundary layer thickness (in)
θ	boundary layer momentum thickness (in)

Subscripts

FR	stagnation point conditions from Fay-Riddell calculation for a hemisphere
Model	specific to the test model
REF	reference condition
∞	freestream static conditions

I. Introduction

The launch of the Space Shuttle Discovery (STS-114) on July 26, 2005 marked the successful execution of NASA's Return-to-Flight Program. This program included the development of new and improved impact-induced damage assessment and analysis tools designed to enhance safety during space operations. Two of the tools that have received extensive use are the Cavity Heating Tool[1] (CHT) and the Boundary Layer Transition Tool[2] (BLTT). The CHT is used to assess local heating augmentation. Locally, the damage to the thermal protection system (TPS) may pass inspection for re-entry without repair; however, the integrated heat load due to premature boundary layer

* Senior Research Engineer, Aerothermodynamics Branch, and AIAA Associate Fellow

transition downstream of the damage may be excessive. The BLTT implements correlations developed to assess this increased possibility, and it includes transition-to-turbulence due to cavity damage[3] and protrusions[4], such as raised gap fillers. Gap fillers have been identified as probable culprits in premature transition onset observed in some Shuttle flights. Application of the BLTT to two protruding gap fillers that occurred during STS-114 required Astronaut Steve Robinson to perform the first on-orbit repair for their removal.

Boundary layer transition, particularly at hypersonic velocities, is a complex, poorly understood fluid dynamic phenomenon.[5] Functionally, it is dependent on geometric shape, boundary surface roughness and waviness, and local fluid flow conditions, as well as environmental issues such as acoustic-induced disturbances. As a result, the descriptive relationships that correlate transition onset contain large uncertainties and typically require a large analysis database for development. As an example, the database used to develop the BLTT correlations contains thousands of wind tunnel runs that were acquired in many conventional hypersonic wind tunnels and impulse facilities. Most of the protuberance data were acquired using pizza-box shaped trips representative of a raised TPS tile. Until recently, only limited centerline fence-geometry data were included in the tool. A sample of the transition heating image data taken from Ref. 6 is presented in Figure 1a where a long throat of transitional flow is visible over the forward 1/4th of the windward surface of the model, followed by the turbulent wedge. *A fully effective trip*, being defined as when the turbulent wedge moves to the fence protuberance location, was not achieved for this run condition. A transition correlation plot of Re_θ/M_e versus $k/\delta(H_e/H_w)^{0.30}$ taken from Ref. 4 is presented in Figure 1b, where H_e/H_w is the enthalpy ratio. The plot compares ground-based data, flight data and correlation curves using "pizza-box" trips and "New Data" from fence-protuberance trip tests. The correlations are presented in a traditional log-log linear format where laminar flow is below the correlation curve and turbulent flow is above. The transition uncertainty is evidenced by the wide spread in the 95% uncertainty curves. Also noted on the chart are the Re_θ/M_e ranges for the present series of transition experiments, highlighting specifically the Mach 10 (M10) range for the present paper.

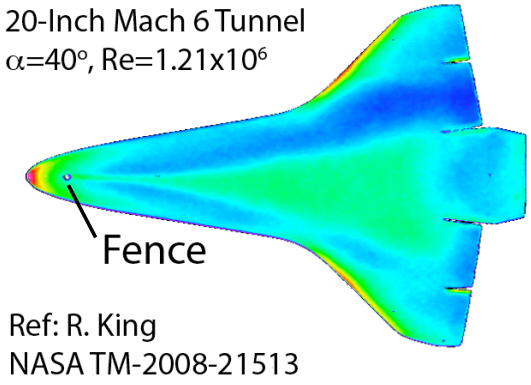

a) Sample transition heating data.

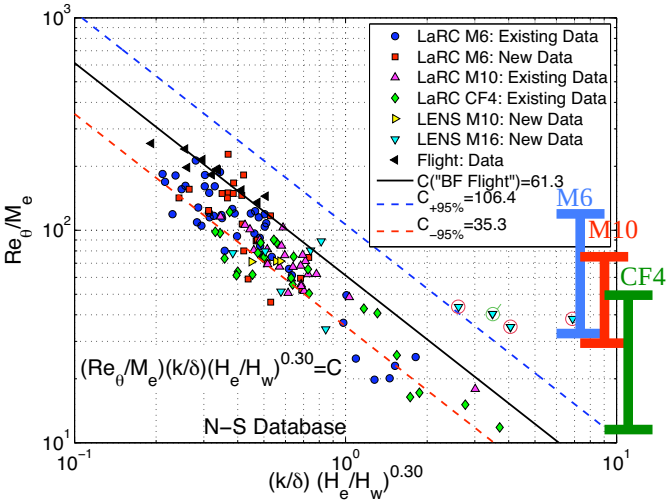

b) Transition correlation (Ref. King, et. al. 2009, Fig. 22).

Figure 1.- Fence-induced transition and correlations.

Extrapolation of ground-based transition correlations to flight conditions introduces significant additional uncertainty because few comparison data exist at the pertinent conditions – controlled, designed flight experiments are almost prohibitively expensive and wind tunnel facilities cannot simultaneously duplicate the required model scales, flow conditions, or energy levels. A recent request to develop a re-entry transition experiment on the Shuttle Orbiter was granted, and to date flights STS-119 and STS-128 have been conducted, with a possibility of others dependent on funding.[7] A newspaper graphic that was originally published in FLORIDA TODAY (March 28, 2009) that describes the experiments is presented in Figure 2. The Shuttle Boundary Layer Transition Flight Experiment (FE) places a 4-inch long by 0.3-inch thick by 0.25-inch high fence on the port wing for STS-119. The fence height H on flight STS-128 was increased to 0.35 inch. Boundary layer state is assessed using the fence-wake surface temperature that is measured via thermocouples embedded in the TPS. Simultaneously, the Hypersonic

Thermodynamic Infrared Measurements (HYTHIRM) Experiment[8] stages a Navy aircraft with a long-range infrared camera along the re-entry trajectory to globally image the transition on the Shuttle surface for comparison. (It should be noted in Figure 2 that the inset view of the protuberance and the temperature sensors are more appropriately representative of a starboard wing installation – the angle of the fence is reversed from the actual flight test article.)

The objective of the present study is to acquire a bounding set of fence-induced transition data on the Shuttle wing in conventional wind tunnels at Mach 6 in air and CF4, and at Mach 10 in air. These data are designed 1) to support further correlation development of the BLTT, 2) to enable comparison with the Shuttle Flight and HYTHIRM measurements, and 3) to support analytical and computational modeling of transition. The specific purpose of this paper is to provide a first look at the transition data acquired on 0.9% scale models of the Shuttle in the Langley 31-Inch Mach 10 Tunnel in air. Presented are a discussion of the test design and scaling, model and fence fabrication considerations, and preliminary data observations. A roadmap of planned testing and data analysis is provided.

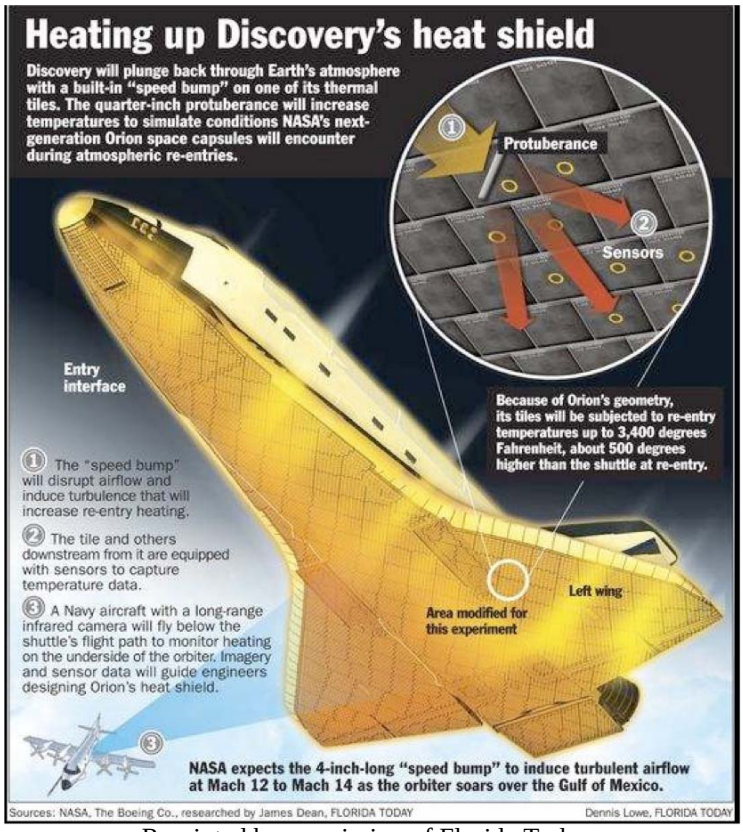

Reprinted by permission of Florida Today.

Figure 2.- The Shuttle Flight and HYTHIRM Experiments.

II. Experimental Methods

This section presents a brief discussion of the experimental methods. The test facility is first discussed, followed by a description of the models and fence design, and an overview of the phosphor thermography data system used to acquire the global heating measurements.

A. Facility

Tests were conducted in the 31-Inch Mach 10 Air Tunnel (M10) at the NASA Langley Research Center (LaRC). This conventional, perfect-gas blowdown facility uses heated, filtered air as the test gas. The tunnel has a square, contoured nozzle, which opens into a 31-inch square test section. Models are supported on a hydraulically operated, sidewall-mounted injection system that can transfer a model from the sealed model box to the tunnel centerline in less than 1 second. Tunnel run times of approximately 60 seconds can be achieved, but typical heating studies that use the global phosphor thermography method require only a few seconds. The nominal reservoir conditions are stagnation pressures of 150 psi to 1450 psi at stagnation temperatures of about 1825˚R. These reservoir conditions very nearly produce perfect gas (γ = 1.4) freestream flows with a Mach number of approximately 10 and unit Reynolds numbers of 0.2×10^6/ft to 2.2×10^6/ft. Micol[9] presents a detailed description of this facility. Flow properties were determined using the GASPROPS code developed by Hollis.[10.]

B. Models

A reference schematic of the windward side of the model is shown in Figure 3. Local flow conditions on the wing, specifically thin boundary layers, and flight-to-tunnel scaling requirements, specifically fence size, dictate using the largest possible models. The M10 has a 10-inch central core at low Reynolds number test conditions[9]. Testing with a sting mount with the model at α=50º (an off-nominal excursion) places the nose near the calibration-determined outer boundary for best flow conditions; the wings will rotate near the tunnel centerline. With these constraints, 0.9-percent scale models (L_{Model}=11.61 inches) of the Shuttle Orbiter were fabricated as follows using ceramic casting methods as described in Buck, et al.[11,12] First, the models were cast from a pattern made using the stereolithographic array process (SLA), and they were partially kiln fired for structural integrity. Fence location marks were then applied at the Flight Test site in the Quality Assurance Laboratory (QA) and fence-rod mounting holes were drilled through each wing normal to the windward surface, providing two test sites per model. The fence design is presented in the next section. A final kiln firing was made to bring the models to test structural strength and the mounting sting was installed through the base. Next, the models were coated with a nominal 27 μm thick mixture of phosphors suspended in a silica-based colloidal binder[13] and returned to QA for measurement and application of small circular indicators, known as fiducial marks. A minimum number of these are used because the marking ink changes the phosphor calibration and this will erroneously alter the local heating measurement. This heating disturbance identifies the fiducial location for use when mapping the two-dimensional heating images to a three-dimensional geometry for data analysis. The final fabrication step is the installation of the fence rods at the prescribed trip height and at the 58º fence-alignment angle. Test data were acquired and the models were again returned to QA for as-tested measurements of the fence heights. It is noted that the vertical tail was not included on these models for ease of fabrication and handling because only wind side heating data were acquired.

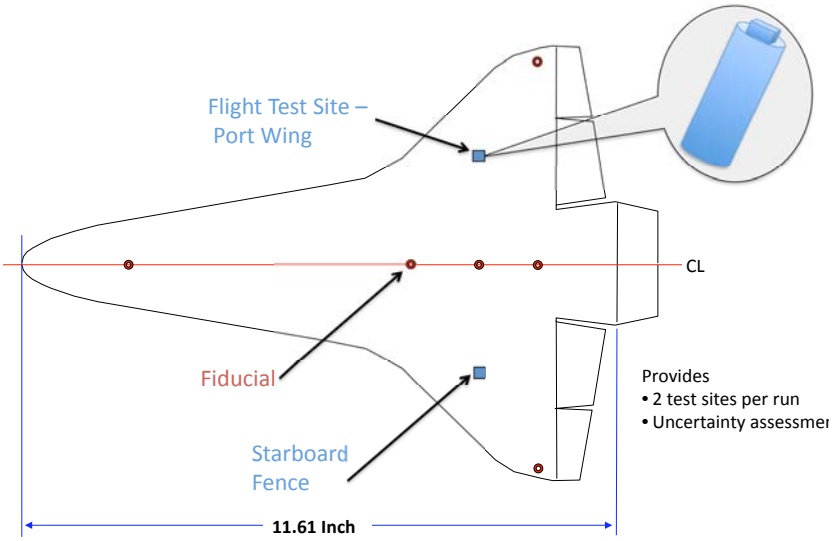

Figure 3.- Schematic of Shuttle test model.

C. Fence Design

Flight-to-tunnel scaling is a significant issue for designing the model-scale fences. The flight-scale fence has nominal dimensions of 4.00 x 0.30 x 0.35 inches that are not feasible to build at a 0.9-percent scale. Therefore, the scaling based on local boundary layer parameters was adopted. The scaled fence geometry at Mach 15 flight conditions was determined using computational predictions of the boundary layer from the LAURA code[14,15] at the flight test site yielding (L_{Fence}/δ, W_{Fence}/δ, H_{Fence}/δ) = (3.478, 0.261, 0.304). Next, the local surface flow conditions at the model fence for α=40º were determined for anticipated tests in the 31-Inch Mach 10 Air, 20-Inch Mach 6 Air, and 20-Inch Mach 6 CF4 Tunnels. Because local boundary layer thickness (δ) decreases and momentum thickness Reynolds number (Re_θ) increases with increasing model Reynolds number, the maximum H_{Fence}/δ and the maximum Re_θ are simultaneously achieved at the highest tunnel pressure. Fence heights were obtained by taking H_{Fence}/δ=1 at the maximum total pressure for each facility. These are given in Table 1, where the

Table 1.- Fence design geometry.

Fence	H_{Fence} (Inch)	Facility
A	0.0050	Low end assessment
B	0.0100	20-Inch Mach 6
C	0.0150	20-Inch Mach 6 CF4
D	0.0175	31-Inch Mach 10
L_{Fence}=0.0323 inches and W_{Fence}=0.0024 inches		

smallest fence labeled **A** was prescribed to parametrically bound the low-end variation of H_{Fence}/δ. Fence length and width geometry was maximized and standardized by using the thinnest boundary layer thickness, δ=0.0093 inches, that occurs for the 20-Inch Mach 6 Tunnel, yielding L_{Fence}=0.0323 and W_{Fence}=0.0024 inches.

Using the two wing test sites provides four different models denoted **AB**, **BC**, **CD** and **DA**, where the initial letter in the naming sequence indicates the port wing installation, corresponding to the flight location. This fence arrangement provides the opportunity for lumped assessment of data uncertainty due to model-to-model fabrication differences, model installation, flow repeatability, and fence fabrication and installation differences. A baseline model without fences is provided in addition to the 4 fence models. Backup models of each were also fabricated.

Fabrication of dimensionally small fence geometries is challenging. Electrical Discharge Machining (EDM) was used to remove excess material on a 0.060-inch diameter drill rod in an attempt to achieve the desired shape. Very highly magnified side and frontal views of sample **B** and **D** trips are presented in Figure 4. The drill rod is on its side in each image with the fence to the right. The EDM process burns away the material and, as a result, leaves a rough and distorted surface. During installation the drill rod is bonded into the model, retracted to achieve the required height, rotated to achieve the correct alignment, and ceramic material is backfilled over the rod if a recession exists. All installation is accomplished under a microscope using filler gages to adjust the height.

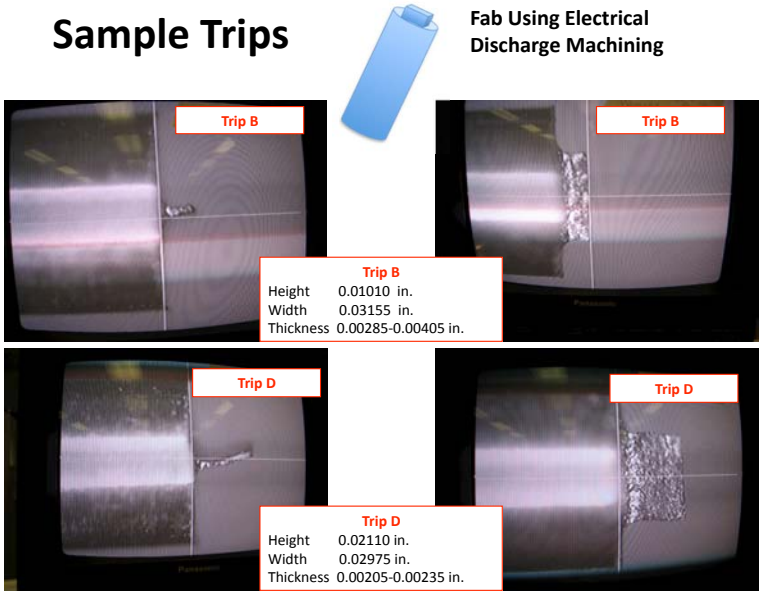

Figure 4.- Highly expanded views of sample fence rods.

D. Phosphor Thermography Technique

Global surface heating distributions were calculated using the two-color, relative-intensity phosphor thermography method.[13] This is the standard technique for obtaining aeroheating data in NASA Langley's hypersonic wind tunnels, and it can be used to identify the surface heating effects of complex three-dimensional flow phenomena, which are difficult to examine using conventional discrete-sensor methods. With this method, ceramic wind tunnel models are coated with phosphor crystals that fluoresce in the red and green regions of the visible light spectrum when illuminated by ultraviolet (UV) light. The phosphor-coated model is exposed to the heated flow during a wind tunnel run, and the resulting changes in fluorescence intensity of the model are recorded and digitized. The surface temperature distributions are determined from the fluorescence intensities through prior calibrations, reduced to surface heating distributions, and analyzed using the IHEAT[13] code, which implements one-dimensional, semi-infinite solid heat conduction theory. These distributions may be mapped onto a 3-dimensional CAD representation of the test article using the MAP3D[13] code or the recently developed iMap code.

III. Data Presentation

This section begins with a qualitative comparison of burn patterns observed downstream of the flight-geometry fence tested on a flat plate in the Johnson Space Center (JSC) Arc Jet with those obtained on an SLA flat-plate model tested in the LaRC 31-Inch Mach 10 Tunnel. This comparison shows near-field flow features that are not readily apparent in the present test because of the small model scale. The initial fence-induced transition data acquired on the Shuttle model in the 31-Inch Mach 10 Tunnel are then presented along with preliminary qualitative observations. This test series encompassed a total of 59 wind tunnel runs. Only data from the **Baseline** model, parameter sensitivity data from model **BC**, and the maximum fence height data from model **CD** will be discussed.

A. Comparison of JSC Arc Jet and LaRC Mach 10 Burn Patterns

The flight fence was tested in the JSC Arc Jet on a Shuttle TPS tile surface.[16] A similar, approximate SLA fence model at 1/10th the scale was tested in the M10 tunnel.[17] The downstream burn patterns resulting from these tests are presented in Figure 5 along with the size of each fence. Even though the Arc Jet provides a much more energetic environment, the similar streaking that marks the surface is evidence of the similarity of the strong vortical structures that develop as the fluid expands around the fence. The enhanced burning and the surface cracks visible on the SLA model are due to the lower temperature capability of the fabrication material, providing clarity in the image. Because of manufacturing constraints, near-field heating data next to the fences installed on the Shuttle models is unavailable. As will be seen, the far-field data will exhibit characteristics similar to those in Figure 5.

L_{trip}	4.00”
W_{trip}	0.30”
H_{trip}	0.35”
L / H	11.43

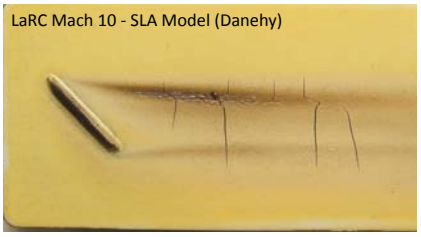

L_{trip}	0.354”
W_{trip}	≈0.039”
H_{trip}	≈0.039”
δ	≈0.039”
L / H	9

Figure 5.- Heating burn patterns on fence geometries.

B. Baseline Model

Installation photographs of the **Baseline Model** that are typical of all models are presented in Figure 6. The model is sting mounted to the support strut. Since the facility has a side injection, the wings are vertical for side viewing with the phosphor thermography data acquisition system camera and for lighting. The large circular disk mounted in the injection window will rotate to allow adjustments to model yaw. Angle of attack adjustments are made at the base of the support strut using a pitch mechanism combined with wedge blocks to extend its range.

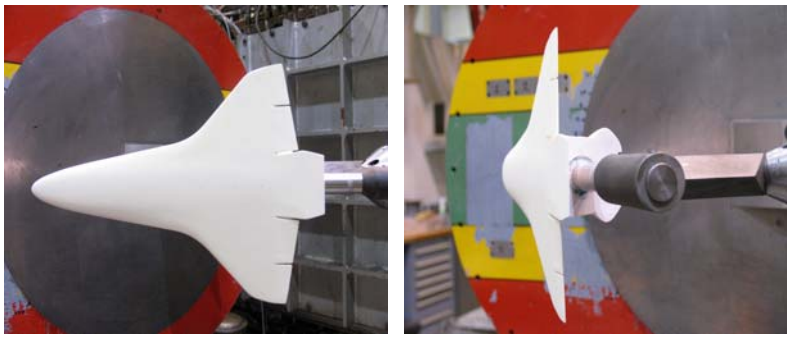

Figure 6.- Baseline model installation.

Representative **Baseline Model** heating data acquired at α=40º are presented in Figure 7 for Re=0.23x10^6 and Re=1.72x10^6. These two Reynolds numbers represent the extreme conditions tested at this angle of attack. The left side of the figure presents the heat images; the center presents the centerline and wing heating distributions; and, the right side presents expanded views of the wing data. Purple on the nose and wing leading edges indicates that the phosphor temperature has exceeded the calibration and is saturated. Local heating, h, is normalized by h_{FR}. The locations of the line cut data are shown on the top left heating image. Very good spanwise symmetry is demonstrated for both test cases as evidenced by the expanded wing plots, indicating symmetry in the cast model fabrication and proper installation. Laminar flow heating levels and distributions are realized over the entire model.

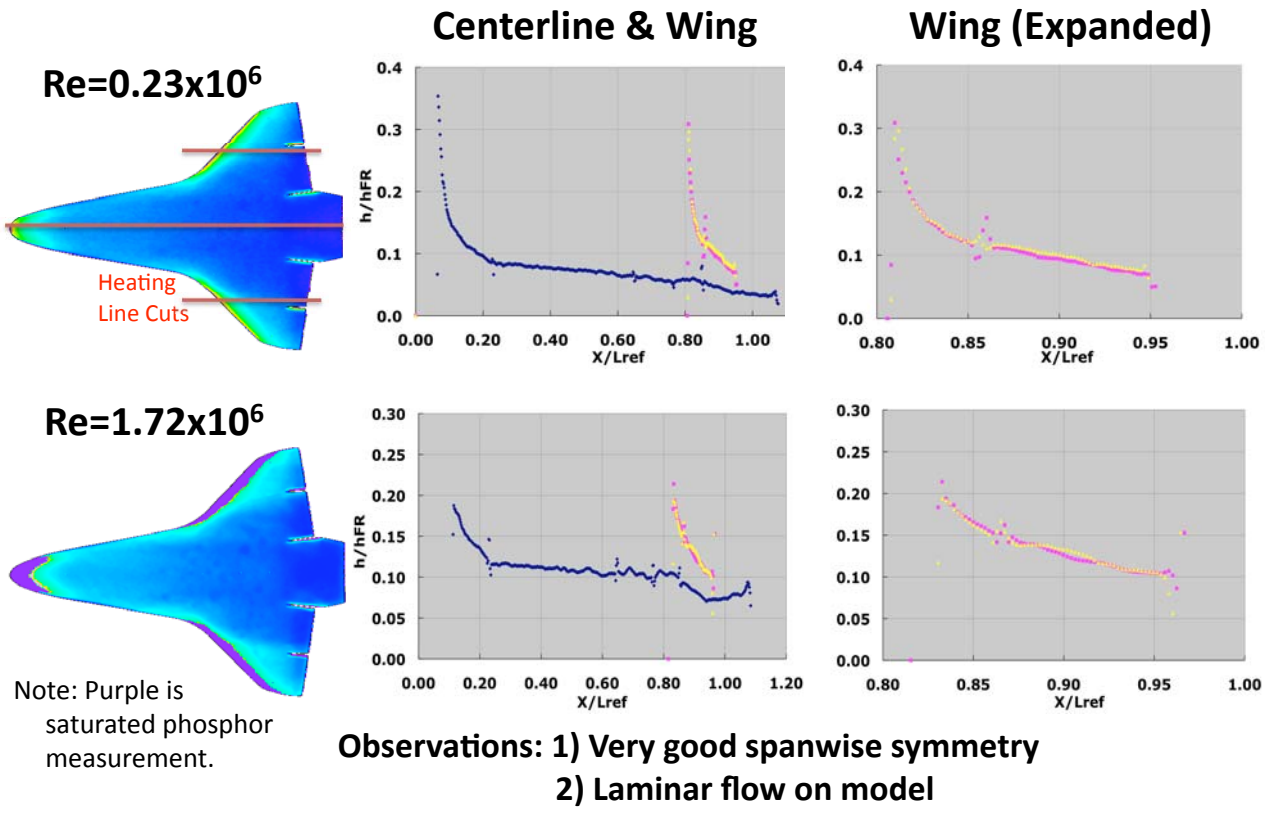

Figure 7.- Baseline Model heating distributions for α=40°.

C. BC Fence Model

The first two fences tested were on the **BC Model** with nominal fence heights of 0.010 and 0.015 inches as shown in Figure 8. Also indicated in the figure are angle alignment fiducial marks along the 58° radial on either side of the fence. As a result of this being the first tested, this is the only model used to perform off-design heating sensitivity variations.

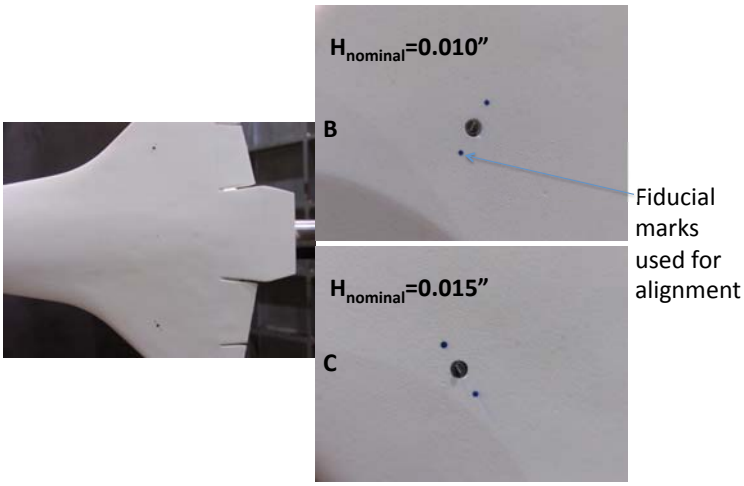

Figure 8.- Model BC fences.

Reynolds number effects at α=40° are presented in Figure 9. Purple heating is again representative of the phosphor measurement being saturated on the nose and wing leading edges. Saturated heating is also present in the fence transition wake at Re=2x10^6, and it serves to highlight the fact the wake remains narrow to the elevon gap and apparently never achieves the fully-effective trip state where a large turbulent wedge is observed at the fence location. As expected, the intensity of the transition wake is decreased as Reynolds number is reduced and the track of the wake is stationary. As will be demonstrated, the transition wedge is similar to that observed in the STS-128 HYTHIRM images.

The influence of α on the transition wake at Re=1x10^6 is presented in Figure 10 As anticipated, the wake moves outboard with increasing angle of attack, responding to the higher inboard pressures. Also observed is the increasing

intensity of the transition wake with increasing α, mirroring corresponding increases in the transition correlation parameter Re_θ/M_e. Again, fully-effective tripping does not appear to have been achieved, even at α=50° where it is most probable.

Proper alignment is important when installing the model. It is also important to understand potential effects of vehicle attitude on transition path in flight. The effects of small changes in sideslip, β, on the transition wake at $Re=1x10^6$ at α=40° are presented in Figure 11. Here, β is varied from -1° to 1°. Little, if any, effects are seen on the transition wake over this range of Δβ.

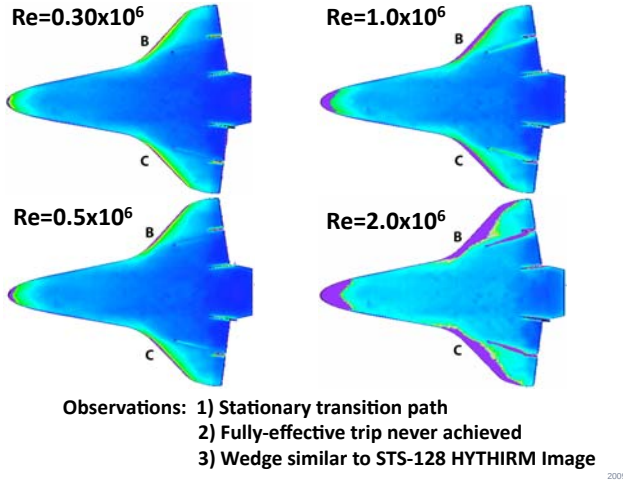

Figure 9.- Model BC — Reynolds number effect at α=40°.

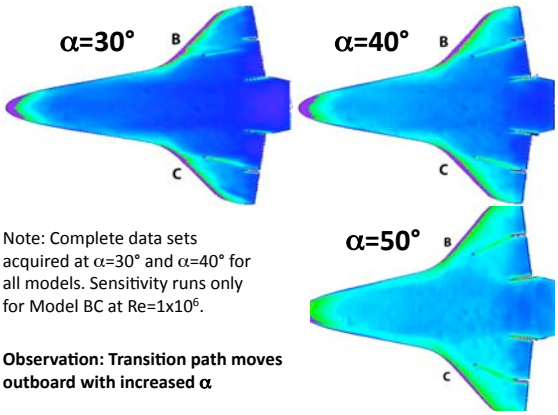

Figure 10.- Model BC — α effects at $Re=1x10^6$.

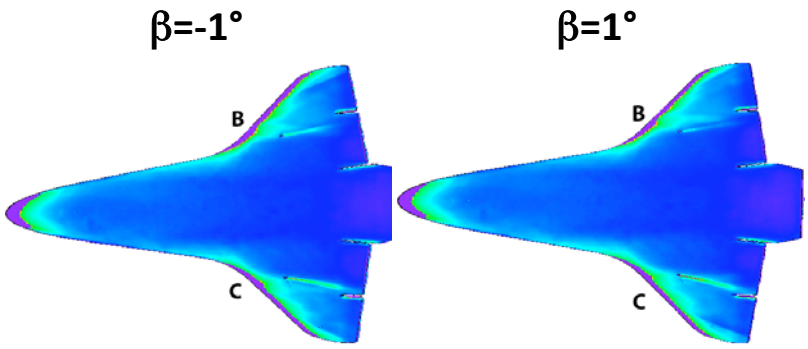

Figure 11.- Model BC — β effects at $Re=1x10^6$. α=40°.

D. CD Fence Model

Close-up images of the **Model CD** fence installations are presented in Figure 12. (For reference, recall that the drill rod has a 0.060-inch diameter.) These represent the largest fence protuberance heights tested. The **C** fence in the top image has been recessed to achieve the desired height and then backfilled with ceramic. Pre-installation side and profile views of the **D** fence were presented in Figure 4.

Heating images showing Reynolds number effects on the **CD** model at α=40° are presented in Figure 13. As with the **BC** model, fully effective tripping at the fence was never achieved as evidenced by the absence of a large turbulent wedge for any of the tested conditions. Because of this, testing was terminated at the completion of **Model CD** — **Model DA** was not tested pending further data analysis and possible increases in fence height.

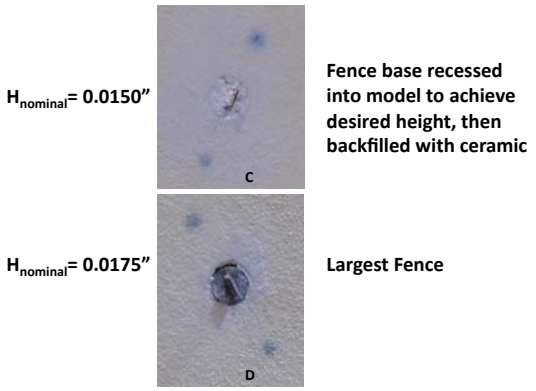

Figure 12.- Model CD fence installation.

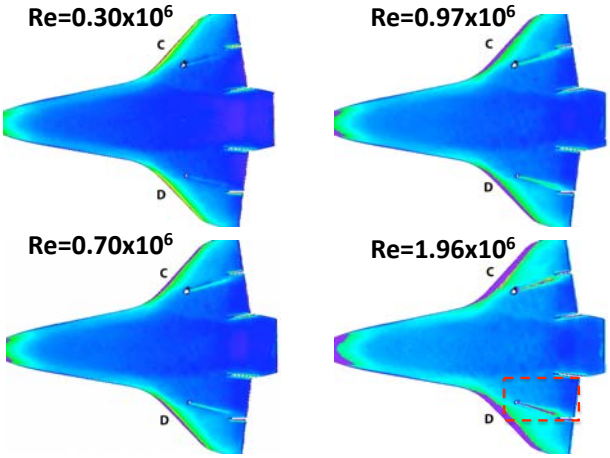

Observation: Fully-Effective transition never achieved with largest fence at M_∞=10 ➔ Model DA not tested.

Figure 13.- Model CD — Reynolds number effects at α=40°.

A close examination of the **D**-fence transition region defined by the dashed box in Figure 13 shows the onset and growth of the turbulent wedge. This region is enlarged and the heating images are presented in Figure 14 with line cut plots of the heating along the transition wake. The transitional heating increases in intensity with Reynolds number and an expansion throat (defined by the sudden wake broadening) is formed between the transitional and the turbulent flows as noted by the arrow at Re=0.97x10^6. The throat position moves linearly upstream with increasing Reynolds number. At maximum Reynolds number, the nominal values of H_{Fence}/δ and of Re_θ/M_e are 0.092 and 125, respectively. Higher values of Re_θ cannot be developed at M10; so, larger values of H_{Fence}/δ and/or higher α (lower M_e) are required to achieve the fully effective trip state.

The near-wake-center line cut plots of the heating shown in Figure 14 begin at the fence (S=0) and end at the elevon flap gap (S=1) along the dashed path as shown in the Re=0.3x10^6 image. They show the typical factor of ≥3 times laminar heating augmentation experienced in turbulent wakes near the throat location. Loss of data integrity is also apparent where the temperatures measured by the phosphor approach and exceed the calibrated range.

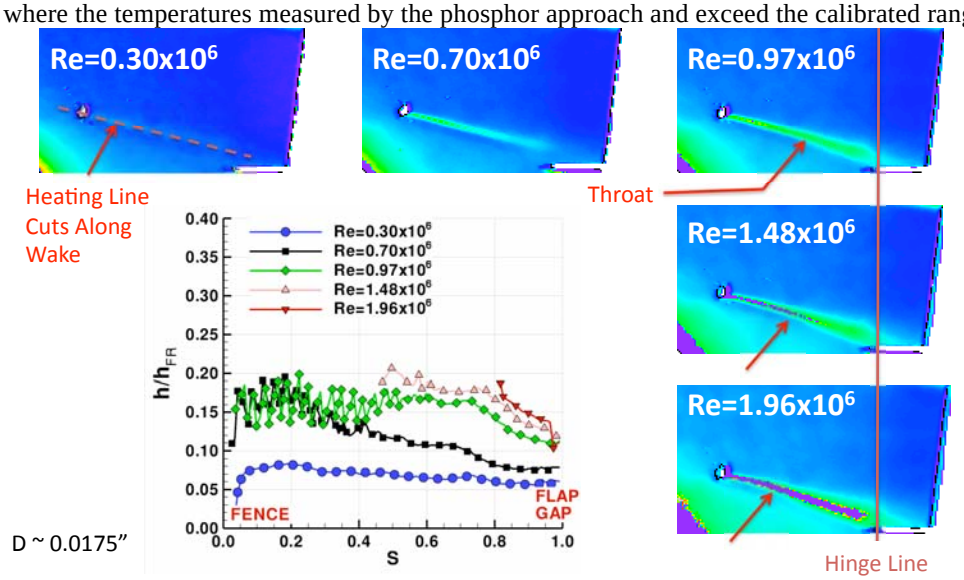

Observation: Questionable whether fully-effective tripping achieved with largest fence at M_∞=10

Figure 14.- D-Fence heating. Reynolds number effect for a=40°.

E. HYTHIRM imagery comparison.

HYTHIRM images obtained during STS-128 on September 11, 2009 are presented in Figure 15. The Mach number is approximately 15. The unprocessed near infrared (NIR) imagery is presented in Figure 15a, clearly showing the heating footprint extending downstream to the trailing edge. A processed temperature image is presented in Figure 15b. Highlighted are the laminar windward flow and the elevon gap heating. The regions of wing leading edge heating are clearly defined, allowing the augmented heating due the fence protuberance to be identified. By symmetry observations, the heating

footprint from the protuberance appears to enter the elevon gap region as it does in the present wind tunnel data. Though still narrow, comparison with Figure 14 indicates a broader disturbance wedge. For reference from the STS-119 trajectory calculations, Re_θ/M_e=109 at Mach 19 and Re_θ/M_e=199 at Mach 13, both significantly greater than the maximum $Re_\theta/M_e \approx 125$ for the present experiments. The augmented body flap heating in flight is a result of the δ=7.5° deflection compared to δ=0° for the wind tunnel.

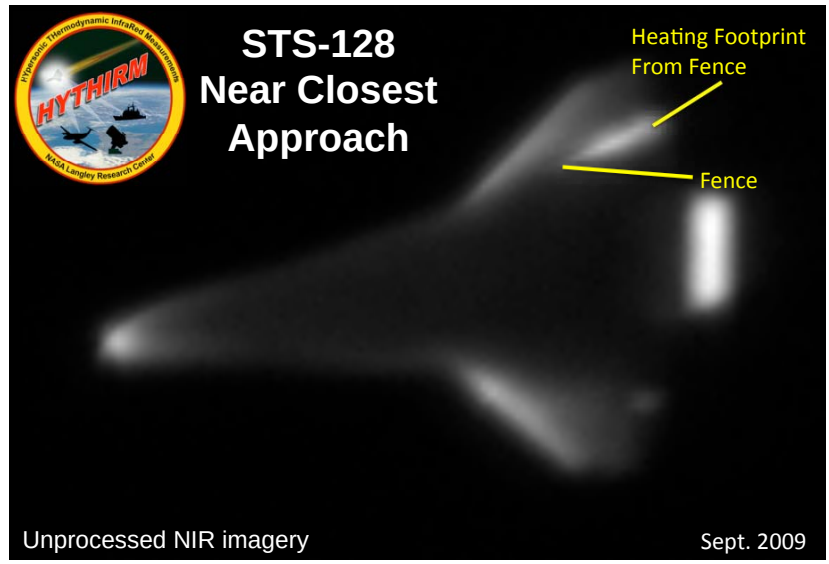

a) Nearest approach.

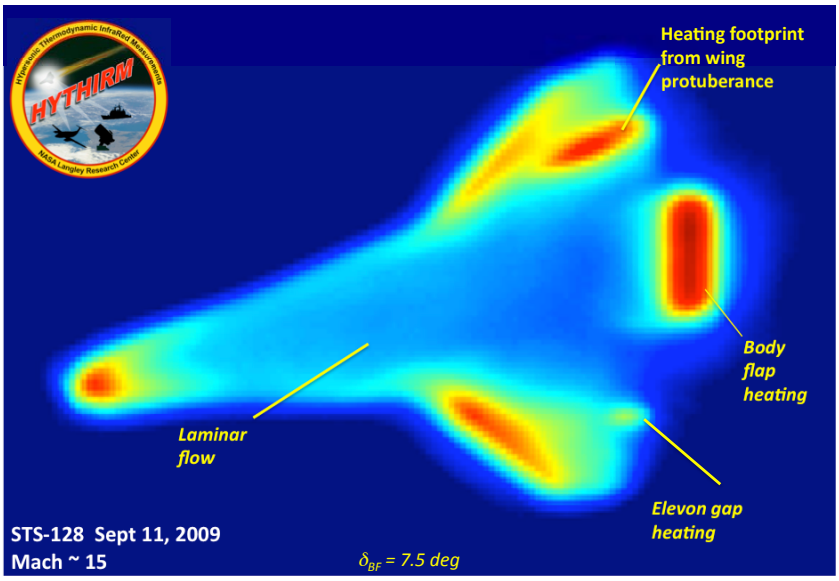

b) Processed imagery.

Figure 15.- HYTHIRM imagery from STS-128.

IV. Concluding Remarks

The data and observations presented here represent a "first look" at recently acquired fence-induced transition on the Orbiter wing at Mach 10. These observations were formed using 2-dimensional heating images obtained via global phosphor thermography. Though not presented, mapping the data from a 2-dimensional image to a 3-dimensional grid was recently completed, enabling detailed analysis to continue and allowing data dissemination. The as-tested fence geometries are currently being measured and evaluated to enable parameter formulation for comparisons with transition correlations used in the *Boundary Layer Transition Tool*. A test in the 20-inch Mach 6 CF4 Tunnel is currently in the planning stage, providing the opportunity to simulate real gas effects and the effects of wall temperature ratio. A test in the 20-Inch Mach 6 Tunnel is anticipated when this facility is returned to operational status to obtain transition results at high-Reynolds number. After examining the present data, a brief return to the 31-Inch Mach 10 Tunnel may be required to address any anomalies or enhance the database.

In summary, fence-induced transition data have been acquired on Shuttle Orbiter models at Mach 10 at the Flight Experiment test site. The data exhibit the expected response to all parameter variations; however, it is questionable whether fully effective tripping was realized at any tested condition with the present model hardware. This boundary

layer state may be achieved in future tests at Mach 10 by increasing fence height to augment the disturbance and/or by increasing angle of attack to reduce the local Mach number, thereby increasing the value of transition parameter Re_θ/M_e. Qualitatively, a preliminary comparison of the ground-based measurements of fence-induced transition at Mach 10 with those obtained from the STS-128 HYTHIRM imagery at Mach 15 reveal similar transition-wake response characteristics in terms of the spreading and the path along the vehicle surface.

V. Acknowledgements

The contributions of Lewis Simmons and Mr. Michael Powers are greatly appreciated for the challenges faced with model fabrication and the difficult fence installations. The excellent work of the Flight and HYTHIRM Teams is evidenced by the STS-128 images provided by Mr. Thomas Horvath.

VI. References

[1] Anderson, Brian, Hyatt, Jay, Wang, K.C., Everhart, Joel, Greene, Frank, Pulsonetti, Maria, Wood, Bill, Bourland, Gary, and Cassady, Amy, "The Cavity Heating Tool," Boeing Technical Memorandum ATA-AH-TM-2005-079, The Boeing Company, NASA Space Systems, Houston, TX, Dec. 7, 2005.

[2] Berry, Scott A., King, Rudolph A., Kegerise, Michael A., Wood, William A., McGinley, Catherine B., Berger, Karen and Anderson, Brian, "Orbiter Boundary Layer Transition Prediction Tool Enhancements," AIAA Paper 2010-246, January 2010.

[3] Kegerise, M. A., King, R. A., and Berry, S. A., "Development of Cavity Induced Boundary-Layer Transition Correlations for Version 2.0 of the BLT Tool," Engineering Note EG-SS-07-05, NASA Johnson Space Center, March 2007.

[4] Rudolph A. King, Michael A. Kegerise and Scott A. Berry, "Version 2 of the Protuberance Correlations for the Shuttle-Orbiter Boundary Layer Transition Tool," NASA TP 2009-215951, November 2009.

[5] Hirschel, Ernst Heinrich,"Basics of Aerothermodynamics," Volume 204, Progress in Astronautics and Aeronautics, Springer-Verlag Berlin, Germany, 2005.

[6] King, Rudolph A., Berry, Scott A., Kegerise, Michael A., "Effect of Protuberance Shape and Orientation of Space Shuttle Orbiter Boundary-Layer Transition," NASA TM-2008-215103, 2008.

[7] Anderson, Brian, Campbell, Charles H., Kinder, Gerald R., and Saucedo, Luis A., "BLT Flight Experiment Overview and In-Situ Measurements," AIAA Paper 2010-0240, 48th AIAA Aerospace Sciences Meeting, Orlando, FL, January 2010.

[8] Horvath, Thomas J., Tomek, Deborah M., Berger, Karen T., Splinter, S., Zalameda, J., Krasa, J., Schwartz, R., Gibson, D., and Tietjen, A., "The HYTHIRM Project: Flight Thermography of the Space Shuttle During Hypersonic Re-Entry," AIAA Paper 2010-0241, 48th AIAA Aerospace Sciences Meeting, Orlando, FL, January 2010.

[9] Micol, J.R.: "Hypersonic Aerodynamic/Aerothermodynamic Testing Capabilities at Langley Research Center: Aerothermodynamic Facilities Complex," AIAA Paper 95-2107, June 1995.

[10] Hollis, B.R., "Real-Gas Flow Properties for NASA Langley Research Center Aerothermodynamic Facilities Complex Wind Tunnels," NASA CR 4755, September 1996.

[11] Buck, G.M., and Vasques, P., "An Investment Ceramic Slip-Casting Technique for Net-Form, Precision, Detailed Casting of Ceramic Models," U.S. Patent 5,266,252, November 1993.

[12] Buck, G.M., Powers, M.A., Nevins, S.C., Griffith, M.S., Verneris, P.H., and Wainwright, G.A., "Rapid Fabrication of Flat Plate Cavity Phosphor Thermography Test Models for Shuttle Return-to-Flight Aero-Heating," NASA TM 2006-214508.

[13] Merski, N.R., "An Improved Two-Color Relative-Intensity Phosphor Thermography Method for Hypersonic Wind Tunnel Aeroheating Measurements," NASA CDTP-1017, February 2001.

[14] Gnoffo, P.A., Gupta, R.N., and Shinn, J.L., "Conservation Equations and Physical Models for Hypersonic Air Flows in Thermal and Chemical Nonequilibrium," NASA TP 2867, February 1989.

[15] Gnoffo, P.A., An Upwind-Biased, Point-Implicit Relaxation Algorithm for Viscous, Compressible Perfect Gas Flows," NASA TP 2953, February 1990.

[16] Roccio, J., "Boundary Layer Transition Protuberance Tests at NASA JSC Arc-Jet Facility," AIAA Paper 2010-1578, , 48th AIAA Aerospace Sciences Meeting, Orlando, FL, January 2010.

[17] Danehy, P.M., Ivey, C.B., Bathel, B.F., Inman, J.A., Jones, S.B., Watkins, N.A., Goodman, K., Leighty, B.D., Lipford, W.K., Jiang, N., Webster, N.M., Lempert, W., Miller, W.J., and Meyer, T., "Orbiter BLT Flight Experiment Wind Tunnel Simulations: Nearfield Flow Imaging and Surface Thermography," AIAA-2010-1571, 48th AIAA Aerospace Sciences Meeting, Orlando, FL, January, 2010.